

Version 2 total ozone mapping spectrometer ultraviolet algorithm: problems and enhancements

Nickolay Krotkov

University of Maryland Baltimore County
Goddard Earth Sciences and
Technology Center
Baltimore, Maryland 21250
and
NASA Goddard Space Flight Center
Laboratory for Atmospheres
Greenbelt, Maryland 20771

Jay Herman

Pawan K. Bhartia

NASA Goddard Space Flight Center
Laboratory for Atmospheres
Greenbelt, Maryland 20771

Colin Seftor

Raytheon ITSS
Lanham, Maryland 20706-4341

Antti Arola

Jussi Kaurola

Sari Kalliskota

Petteri Taalas

Finnish Meteorological Institute
Helsinki, FIN-00101
Finland

Igor V. Geogdzhayev

NASA Goddard Institute for Space Studies
and
Columbia University
New York, New York 10027

1 Introduction

Potential global increases in UVB irradiances from decreasing stratospheric ozone amounts^{1–13} caused by anthropogenic release of chlorine gases (mostly chlorofluorocarbons) have been an issue of public concern for the past 20 years, because of their impact on human health as well as terrestrial and aquatic ecosystems.^{14–20} Several satellite-based methods for estimating UV irradiance have been suggested.^{4,8,21–37} Because of their long time record and global contiguous spatial coverage, two NASA total ozone mapping spectrometer (TOMS) data³⁸ are used for estimating global trends in surface UV irradiance^{4,8,24} and studying global UV climatology^{28,31} (especially for land regions not covered by ground-based UV networks and over oceans^{39,40}). The TOMS UV record will continue with the hyperspectral ozone monitoring instrument⁴¹ (OMI to be launched in 2004 on the NASA EOS/Aura satellite) as the successor to TOMS.

TOMS estimation of UV irradiance using the current Version 1 algorithm is usually larger than ground-based

Abstract. Satellite instruments provide global maps of surface UV irradiance by combining backscattered radiance measurements with radiative transfer models. The accuracy of the models is limited by uncertainties in input parameters representing the atmosphere and the Earth's surface. To reduce these uncertainties, we have made enhancements to the currently operational TOMS surface UV irradiance algorithm (Version 1) by including the effects of diurnal variations of cloudiness, an improved treatment of snow/ice, and a preliminary aerosol correction. We compare results of the version 1 TOMS UV algorithm and the proposed version. We evaluate different approaches for improved treatment for average cloud attenuation within a satellite pixel, with and without snow/ice on the ground. In addition to treating cloud transmission based only on the measurements at the local time of the TOMS observations, the results from other satellites and weather assimilation models can be used to estimate atmospheric UV irradiance transmission throughout the day. A new method is proposed to obtain a more realistic treatment of the effects from snow-covered terrain. The method is based on an empirical relation between UV reflectivity and measured snow depth. The new method reduces the bias between the TOMS UV estimations and ground-based UV measurements for snow periods. We also briefly discuss the complex problem of estimating surface UV radiation in presence of UV-absorbing aerosols. The improved (Version 2) algorithm can be applied to reprocess the existing TOMS UV irradiance and exposure estimates (since November 1978) and to future satellite sensors (e.g., GOME-2, OMI on EOS/Aura, and Triana/EPIC). © 2002 Society of Photo-Optical Instrumentation Engineers. [DOI: 10.1117/1.1519541]

Subject terms: UV irradiance; TOMS; radiative transfer models; aerosols; clouds; snow albedo.

Paper UV-003 received Apr. 14, 2002; revised manuscript received June 20, 2002; accepted for publication June 21, 2002.

measurements for most locations in the northern hemisphere (~10% station-average overestimation under snow-free conditions^{31,42–45}), while frequently underestimating the irradiance in the presence of snow.⁴⁶ Part of this bias can be attributed to the current (Version 1) TOMS UV algorithm (mostly from inadequate treatment of aerosols) and part to ground-based instrument problems. The goal of this work is to describe planned improvements to the operational TOMS UV algorithm^{23,27,31,36,41} that will reduce this bias. The proposed improvements will only be implemented after an extensive validation period. The improved (Version 2) UV algorithm will be shared between TOMS (1979 to the present) and future GOME-2, TRIANA/EPIC, and OMI UV products.

2 Overview of the Current TOMS UV Algorithm

The amount of ultraviolet radiation in the UVA (320 to 400 nm) and UVB (290 to 320 nm) spectral regions that reach the surface of the Earth is determined by Rayleigh scattering from the molecular atmosphere, the absorption of

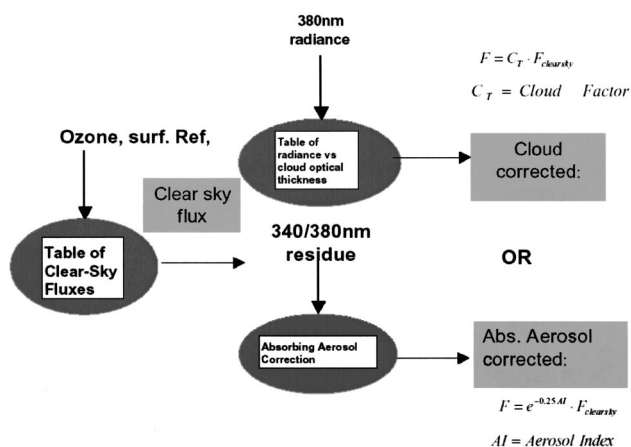


Fig. 1 TOMS Version 1 UV algorithm processes diagram.

ozone, scattering by clouds, and both scattering and absorption by aerosols.^{5–13} The current TOMS UV algorithm (Version 1) is based on corrections to calculated clear-sky UV irradiance, E_{clear} . The estimation procedure is based on table lookup and either cloud/nonabsorbing aerosol correction³⁶ or absorbing aerosol correction^{27,31} (Fig. 1):

$$E_{cloud} = E_{clear} C_T \quad (1)$$

According to Eq. (1), C_T is a relative atmospheric transmittance for global (direct plus diffuse) irradiance normalized to the cloud- and aerosol-free atmospheric transmittance. As previously described in the literature,^{27,31} calculation of E_{clear} in the UV spectral range is obtained from satellite-derived spectral extraterrestrial solar irradiance^{47–50} and TOMS measurements of total column ozone and surface reflectivity.³⁸

In the absence of snow, clouds, and aerosols, the effects of molecular (Rayleigh) scattering, ozone absorption, solar zenith angle, and altitude are well-understood problems. However, the presence of aerosols,^{51–56} clouds,^{5,10,13,21–36} and snow^{57–59} in the satellite field of view (FOV) requires additional corrections. Exact corrections would require the complete characterization of the optical state of the atmosphere and the Earth's surface during the course of the day (for daily exposure calculations). Since complete information is never available from the satellite data alone, the correction factor (C_T) for irradiance has to be estimated using limited information available from the single satellite measurement at the overpass time. The type of correction (specific C_T algorithm) is selected based on the two threshold values of the aerosol index (AI) (calculated from 340 and 380-nm radiances in the case of Nimbus 7 TOMS and from 331 and 360 nm in the case of Earth Probe TOMS) and Lambertian equivalent reflectivity (LER) (360 or 380 nm). The surface albedo and snow effects are estimated using the TOMS monthly minimum Lambertian effective surface reflectivity ($R_M = MLER$) global database^{60,61} as described in Refs. 36 and 41. Table 1 includes estimates of the various error sources in E_{cloud} . In addition to the uncertainties in estimated irradiance at the overpass time, there is additional uncertainty in the estimated daily UV exposure.⁴⁵ The TOMS UV algorithm (Version 1) estimates daily exposure, assuming no diurnal changes in cloud or aerosol properties. The next section discusses possible improvements to this assumption.

3 Improved Cloud Correction for UV Exposure

Clouds are the main cause of short-term UV daily exposure variability at a given geographic location. Information obtained from a single polar orbiting satellite is usually limited to one daily low-resolution UV reflectance measure-

Table 1 Estimated errors in TOMS/OMI spectral UV irradiance including uncertainty in UV extraterrestrial solar irradiance.^{a41}

Atmospheric scenario	305 nm	310 nm	324 nm	380 nm
Background, snow free	10%	8%	7%	6.5%
Seasonal snow (10% rms) ^b	27%	26%	25%	25%
Permanent snow (3% rms) ^c	30%	30%	30%	30%
Episodic events				
Smoke plume ^d	22%	21%	21%	22%
Desert dust plume ^e	15%	13%	11%	15%
Urban pollution ^f	20% (30%)	15% (25%)	10% (20%)	10% (15%)

^aEffects of subpixel variability are not considered.

^bAssuming 10% uncertainty in snow albedo rms and 2.5 amplification factor for average snow albedo 0.5.

^cAssuming 3% uncertainty in permanent snow albedo rms and 10 amplification factor for snow albedo 0.9.

^dTOMS absorbing aerosol index method applied assuming 20% smoke model uncertainty at 324 nm and 5% smoke height uncertainty. Additional spectral transmittance uncertainty is estimated as 5% at 305 nm, 2% at 310 nm, and 6% at 380 nm.

^eTOMS Absorbing Aerosol Index method applied assuming 5% dust model uncertainty at 324 nm and 10% dust height uncertainty. Additional dust spectral transmittance uncertainty is estimated as 10% at 305 nm, 5% at 310 nm, and 10% at 380 nm.

^fMexico City aerosol climatological scenario for typical (annual average) aerosol loading.⁷² Numbers in parenthesis apply to extreme pollution events.

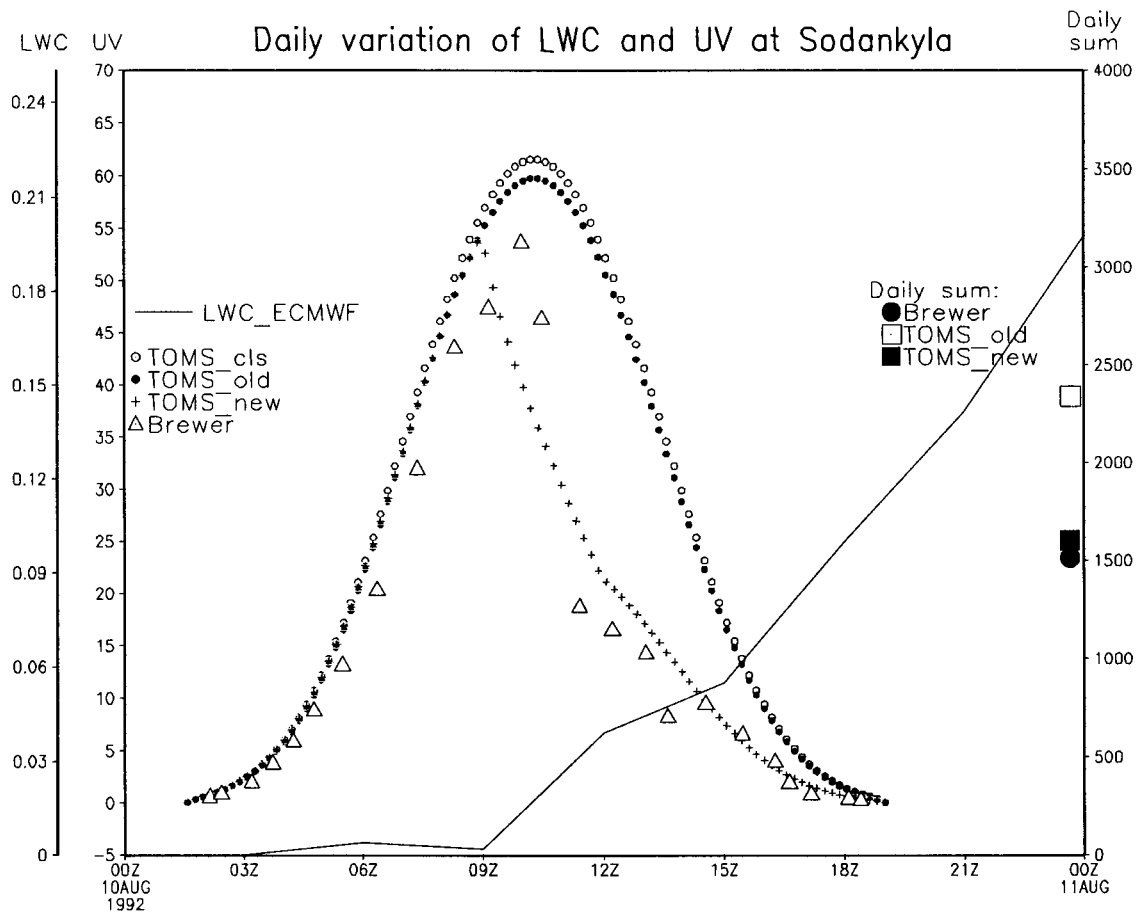


Fig. 2 Comparison of original and improved cloudiness treatment in the UV algorithm. Liquid and ice water data of ECMWF (solid line) is used (assuming total overcast case) in the improved case. The improved method [Eq.(5)] shows better agreement with the Brewer daily observations (diamonds), whereas the original TOMS algorithm [Eq.(3)] gives an overestimate of the daily dose $\sim 60\%$ for this particular case.

ment (FOV ~ 100 km for TOMS and ~ 50 km for OMI and GOME-2) at a given location (except at high latitudes). For the low resolution FOV, it is only necessary to calculate an average scene cloud transmission. The TOMS UV algorithm uses a homogeneous cloud model embedded in a Rayleigh scattering atmosphere with known ozone absorption and known surface reflectivity, A_S , assuming 100% cloud cover in the model.^{36,41} For snow-free conditions A_S at 360 or 380 nm is low (~ 1 to 10%) and can be accurately predicted from a global minimum reflectivity database that was developed using 15 years of TOMS data.⁶⁰ The same database is currently used for regions that can have snow cover (see detailed discussion later on), when a snow/ice climatology indicates that there should be snow/ice for a given location and day of the year. The reflectivity database is currently being revised to 360 nm for both Nimbus and Earth-probe/TOMS. Assuming that A_S is known, the “effective” cloud optical thickness $\tau(t_0)$ is derived by matching the measured 360-nm radiance at the overpass time, t_0 , with the precalculated radiance for each TOMS FOV. The same cloud model is used to calculate the FOV average cloud transmittance, C_T , as a function of $\tau(t_0)$, A_S , and

solar zenith angle θ_0 , at the overpass time and all UV wavelengths, assuming spectrally independent τ and A_S :

$$C_T(\lambda, t_0) = C_T[\lambda, \tau(t_0), A_S, \theta_0(t_0)] \quad . \quad (2)$$

The spectral independence of τ for pure cloud scattering is an accepted approximation in the near UV spectral region (300 to 400 nm), and was confirmed by Mie calculations.^{53,61} The current TOMS UV algorithm also neglects the spectral dependence of A_S , which is less than 0.05 over both land and ocean^{40–41,62} in the UVA and UVB spectral regions (300 to 400 nm). Even with spectrally independent τ and A_S , the method accounts for the spectral dependence of C_T that results from reflection between the cloud and the atmosphere, as well as multiple reflections between the cloud and the surface.³⁶

To calculate daily exposure, the diurnal variation of $C_T(\lambda, t)$ is estimated from changes in the solar zenith angle, assuming a fixed value of cloud optical thickness: $\tau(t) = \tau(t_0)$:

$$C_T(\lambda, t) = C_T[\lambda, \tau(t_0), A_S, \theta_0(t)] \quad . \quad (3)$$

Obviously the assumption of “frozen” near-noon cloud optical thickness will usually lead to an incorrect UV-exposure estimate for any given day (Fig. 2). Since the error might be of either sign, the “sampling bias” may be significantly reduced in cumulative UV monthly exposures at least for some locations. The sign and magnitude of the monthly/yearly sampling bias depends on local cloud diurnal statistics and satellite overpass time. This type of error does not apply to near-noon irradiance estimates from satellite observations (Table 1).

3.1 Assimilating the ECMWF Water Content to Construct a Time-Resolved Homogeneous Cloud Model

To improve daily exposure estimates, additional cloudiness information per day is needed. Such information is available from global analyses made by operational weather forecasting centers and from geostationary satellites (GOES, Meteosat³²). Specifically, one can use vertically integrated cloud parameters [total cloud cover $T_C(t)$, and total column water and ice content $LWC(t)$] provided by a numerical model, normalized to the TOMS $C_T(t_0)$ at the overpass time. For example, global ground-based, balloon borne, and satellite weather observations are used for producing global 3-D analyses by the European Centre for Medium-Range Weather Forecasts (ECMWF) operationally every 3 h. In this study we use an ECMWF Era-15 reanalyzed dataset (1978 to 1994) (<http://www.ecmwf.int/research/era/ERA-15/>), which is concurrent with the Nimbus 7 TOMS data. In the Era-15 dataset, analyses are available every 6 h. To have cloud parameters every 3 h, short three-hour forecasts starting at each analysis time were also used. The spatial resolution of Era-15 data is about 1.6 deg in latitude and longitude, which is much coarser than the resolution of the current operational analyses by ECMWF. The development of the following methods were done using a TOMS grid (1×1.25 deg), therefore the Era-15 data was interpolated to this grid.

The easiest way of assimilating the model parameters into the TOMS UV operational processing algorithm is to scale TOMS effective cloud optical thickness proportionally to the diurnal changes of the ECMWF cloud optical thickness, τ_E , estimated from the model total column water and ice content, $LWC(t)$, assuming a homogeneous cloud layer with C1 droplet size distribution⁶³ (the same as in the Version 1 TOMS UV algorithm).

$$C_T(\lambda, t) = C_T[\lambda, \tau(t), A_S, \theta_0(t)] \quad (4)$$

$$\tau(t) = \tau_0(t_0) \frac{\tau_E(t)}{\tau_E(t_0)}.$$

This algorithm becomes computationally unstable when $LWC(t_0)$ [and $\tau_E(t_0)$] approaches zero or there are large disagreements between the model and TOMS estimates of the cloud optical thickness at the overpass time. In such cases, the following computationally stable algorithm can be used:

$$\tau(t) = \tau(t_0) + \tau_E(t) - \tau_E(t_0). \quad (5)$$

We note that Eq. (5) reduces to Eq. (4) if the TOMS and model optical thickness agree at the overpass time: $\tau(t_0) = \tau_E(t_0)$. The scheme also works when either $\tau(t_0) = 0$ or $\tau_E(t_0) = 0$. If TOMS and ECMWF values are far apart at the overpass time (which is not uncommon), Eq. (5) gives more reasonable values of cloud optical thickness than Eq. (4).

An example of the methodology is shown in Fig. 2, which shows the daily evolution of $LWC(t)$ and UV radiation as measured by a Brewer instrument on 10 August 1992 at Sodankylä (Finland, latitude 67.37°N). According to the model (and SYNOP observations), both T_C and $LWC(t)$ increased during that day. The UV dose rates calculated with the old [Eq. (3)] and new [Eq. (5)] versions of the TOMS UV algorithm are shown with approximately 10-min time steps. The dose rates calculated by the original algorithm [closed circles, Eq. (3)] closely follow the clear-sky dose rates (open circles) because the overpass time ($t_0 = 8$ UTC) was almost cloud-free. As a result, the original method overestimates the daily UV dose by 60% as compared to the ground-based data, while the new algorithm gives a satellite estimate of daily exposure [Eq. (5)] that is close to the observation.

The proposed daily exposure cloud algorithm was tested using combined noontime TOMS and 3-h ECMWF data for summer 1992 at Sodankylä (Fig. 3). The overall performance of the new algorithm is better than the old one. The mean difference between the TOMS UV and Brewer data is reduced from 182 J/m² to 126 J/m² during the period, at the same time correlation increased from 0.86 to 0.89. The specific improvement in cloud algorithm (i.e., C_T) is even better than the absolute numbers indicate, since a substantial portion (about half) of the current bias between the TOMS and the Brewer measurements is not related to the TOMS cloud algorithm.³¹

These results present a first-guess implementation using only water content time-resolved cloud data from the ECMWF model. Fine tuning of the cloud algorithm will be performed to improve the agreement between the observed and the improved cases further. In the TOMS UV project, the global comparability between different cloud models will be studied (i.e., ECMWF, NOAA-NCEP, NASA-Goddard, and NASA-ISCCP models), and improvements in the methodology will be made as needed. For example, we plan to compare cloud data from the ECMWF model with the similar data from International Satellite Cloud Climatology Project (ISCCP <http://isccp.giss.nasa.gov/>) when both are available. ISCCP analysis combines satellite-measured radiances from geostationary and polar satellites with ice/snow data to obtain information about clouds (optical depth and cloud fraction) and the surface.⁶⁴ Pixel analysis is performed separately for each satellite radiance dataset and the merged results are reported in the Stage DX data product with nominal resolution of 30 km and 3 h. Using ISCCP data operationally for TOMS processing is currently impossible because of the large time delay in releasing ISCCP data products. The ISCCP data may be used for future reprocessing of the global TOMS UV-exposure maps. We will also analyze the possibility of using TOMS ozone and high-resolution satellite time-resolved cloud information to produce regional UV maps and overpass

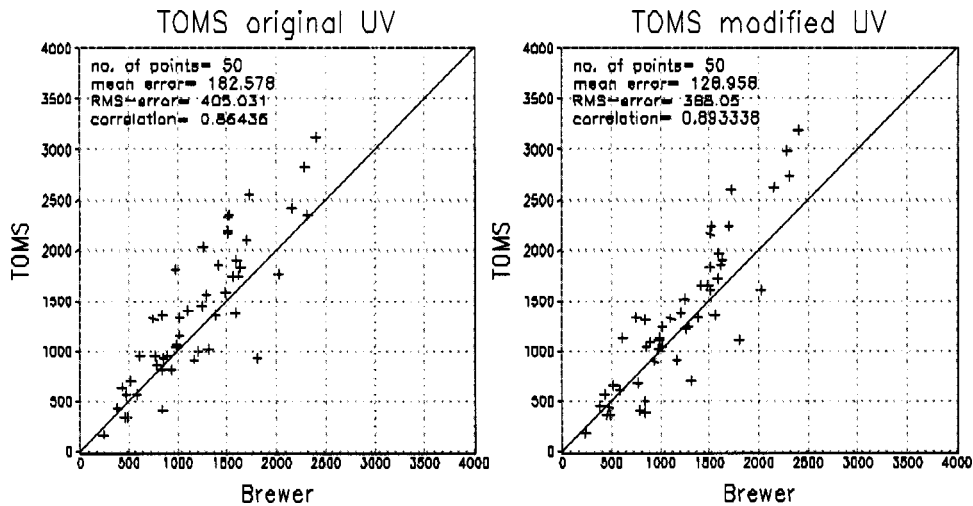


Fig. 3 Comparison of daily erythemal (CIE) UV doses [J/m^2] calculated with original [Eq.(3)] and improved [Eq.(5)] cloudiness treatment in the TOMS UV algorithm with ground-based Brewer observations at Sodankylä from 8 July to 1 September 1992.

datasets. One possibility is to use Meteosat Second Generation (MSG) Climate SAF products for producing UV maps over Europe and Africa,³² and NOAA-GOES data for US and South America coverage.

3.2 Combining the ECMWF Cloud Fraction and Water Content with the TOMS C_T

One of the factors in the overestimation of the TOMS UV data for high irradiance levels (Fig. 3) may be related to the broken-cloud effects. The ECMWF model can be combined with the fractional cloud model,⁶⁵ since it contains the cloud cover information $T_c(t)$. We study the possibility of using both T_c and water content information from the model to improve estimation of C_T . For areas where there are ground-based measurements or a region of specific biological interest, the cloud pattern data from high resolution satellite images (ATSR-2, AVHRR, SeaWiFs, and geostationary satellites, e.g., GOES) can also be used to estimate true cloud fraction $T_c(t_0)$, so the C_T cloud model data can be adjusted. To assimilate both ECMWF cloud parameters, they first should be normalized using the TOMS radiance measurement at the overpass time:

$$I^{\text{Measured}}(t_0) = T_c(t_0)I_{\text{cloud}}^{\text{Calc}}[\tau_F(t_0)] + [1 - T_c(t_0)]I_{\text{clear}}^{\text{Calc}}. \quad (6)$$

Here $\tau_F(t_0)$ is the effective optical depth of the cloud portion of the TOMS FOV, derived from the TOMS measured radiances by table lookup at the overpass time. Next, the ECMWF model time-resolved cloud data, normalized by the $T_c(t_0)$ and $\tau_F(t_0)$, can be used to predict diurnal variation of $C_T(t)$, in a manner similar to Eq. (4):

$$C_T(t) = 1 - T_c(t)\{1 - C_T[\lambda, \tau_F(t), A_S, \theta_0]\}. \quad (7)$$

The fractional cloud model described here still ignores the 3-D cloud structure and related cloud-radiation effects (cloud shadows, reflection from nonhorizontal surfaces) that are discussed briefly in Sec. 7 in the Appendix. The broken cloud model will also be combined with tropo-

spheric aerosol models to study combined cloud/aerosol/radiation interactions. Before adopting either of these approaches in the Version 2 TOMS UV algorithm, we will perform validation studies using radiative transfer modeling and comparisons with ground-based UV data for selected stations.

4 Snow Effects

A major problem using satellite data to estimate UV irradiance at high latitudes arises from the difficulty in identifying the presence of clouds when there is snow on the ground. When TOMS views a scene containing ice, snow, and clouds, there is no way to separate the effects of snow from clouds based on one reflectivity measurement. However, if the surface reflectivity (albedo) A_S is established for various conditions in a geographical region, the excess scene reflectivity can be used to estimate cloud transmittance, C_T , over a snow surface.^{36,41} The current TOMS UV algorithm uses the monthly minimum Lambert equivalent surface reflectivity ($R_M = \text{MLER}$) global database^{60,61} to estimate A_S at 360 or 380 nm. The algorithm also assumes that A_S does not change with wavelength in the UVA and UVB spectral regions. Over land, these assumptions are in reasonable agreement with direct ground-based measurements of UV albedo.^{57–59,66,67} MLER is a reasonable estimate of the surface albedo for either snow-free conditions or regions with permanent snow cover (Antarctica, Greenland). However, MLER is not a good estimator of actual surface albedo during seasons when surface albedo varies daily, depending on the presence and state of snow cover.

In the absence of actual snow information, the current TOMS algorithm uses a climatological snow/ice flag (probability of the presence of snow on a given day at a given location) to estimate the presence of snow. If snow is anticipated, the algorithm first determines a snow albedo threshold (SAT). Currently the SAT is simply the MLER value bounded from below by a constant value of 0.4. The value 0.4 was selected as appropriate for snow covered urban/suburban populated areas containing at least moder-

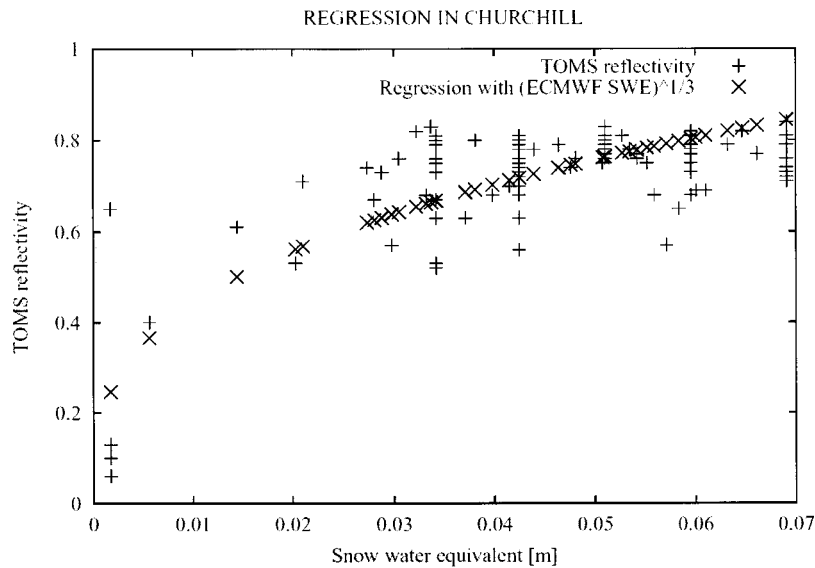


Fig. 4 Statistical relationship (regression) between snow depth and regional snow albedo estimated from the TOMS reflectivity measurements (50×50 km) on cloud-free days with snow at Churchill, Canada.

ate densities of roads, houses, and trees (e.g., Toronto, Moscow).^{36,41} The daily estimation of A_S is based on the comparison of SAT with the actual TOMS measured reflectivity (LER) at 360 nm. If LER is less than (SAT+0.05), the cloud-free conditions are assumed and A_S is set equal to LER ($C_T=1$). If LER is more than SAT+0.05, A_S is set equal to SAT and all additional measured reflectivity is assigned to a cloud above the snow surface. The algorithm proceeds to the calculation of the effective cloud optical thickness and C_T as described before.

The constant threshold value 0.05 was chosen because of the difficulty in detecting thin clouds over snow surfaces. This problem is worse at high latitudes over areas with permanent snow cover (Greenland, Antarctica). For such regions, the possible error in cloud correction could exceed the error due to neglect of the clouds.^{36,41} Therefore, cloud-free conditions are also assumed if the SAT value is more than 0.9. On average, the current TOMS algorithm leads to underestimation of UV radiation in winter conditions.^{35,37,46}

To obtain a more realistic treatment of the albedo of snow-covered terrain, a new method was developed.⁶⁸ This method is based on an empirical relation between UV reflectivity and snow depth. To establish such a relation, cloudless days with snow cover were selected based on the total cloud cover and snow depth (SD) parameters from the ECMWF ERA-15 reanalysis dataset (covering the time period 1979 to 1994). These data, together with the coincident and colocated Nimbus 7 TOMS reflectivity measurements, were used to develop regression models for each ground pixel according to the following equation:

$$R = u \times SD^\gamma, \quad (8)$$

where R is the measured TOMS reflectivity for a given site on cloud-free days with snow, SD is the snow water equivalent, and u is a fit parameter, specific to each grid point and γ is a global fit parameter.⁶⁸ Figure 4 shows an

example of the regression for Churchill, Canada, from which the parameter u was estimated. Similar regressions were obtained for each global grid point. In the future, the snow depth information could be obtained on the same day of satellite radiance acquisition from the models or other satellites. Then the actual snow albedo, A_S , can be calculated from Eq. (8) for each ground pixel and used (instead of MLER) in satellite-retrieved UV calculation of E_{clear} [Eq. (1)] and C_T [Eq. (3)]. Figure 5 shows a comparison of the proposed method with the current MLER algorithm for Sodankyla, Finland and Churchill, Canada. As expected, this method improved the correspondence between the satellite-retrieved results and ground-based measurements, particularly during the melting period in those locations where the regional snow albedo is high.

5 Aerosol Effects

For the purposes of estimating UV irradiance at the Earth's surface, there are two major classes of aerosols that must be considered: aerosols that only scatter UV radiation, and aerosols that both scatter and absorb UV radiation. The first category is included in the measured scene reflectivity (cloud optical thickness), and attenuates UV radiation in a manner that approximates clouds of equivalent reflectivity. However, since these aerosols decrease the direct solar radiation but increase the diffuse radiation, they have relatively small effect on the total surface UV irradiance.²⁷ Moreover, satellite UV instruments can see the increase in the reflected radiation and correct for it. Typical attenuation by such aerosols ranges between 1 and 10%. Though the operational (Version 1) TOMS UV algorithm does not distinguish between water clouds, haze, ice clouds, and non-absorbing aerosols, for a nominal aerosol optical thickness of 0.5 at 380 nm, the error in estimating the UV attenuation by these various sources is $\sim 1\%$.⁴¹

By contrast, aerosols that absorb the UV radiation attenuate both the direct and diffuse radiation, so the surface

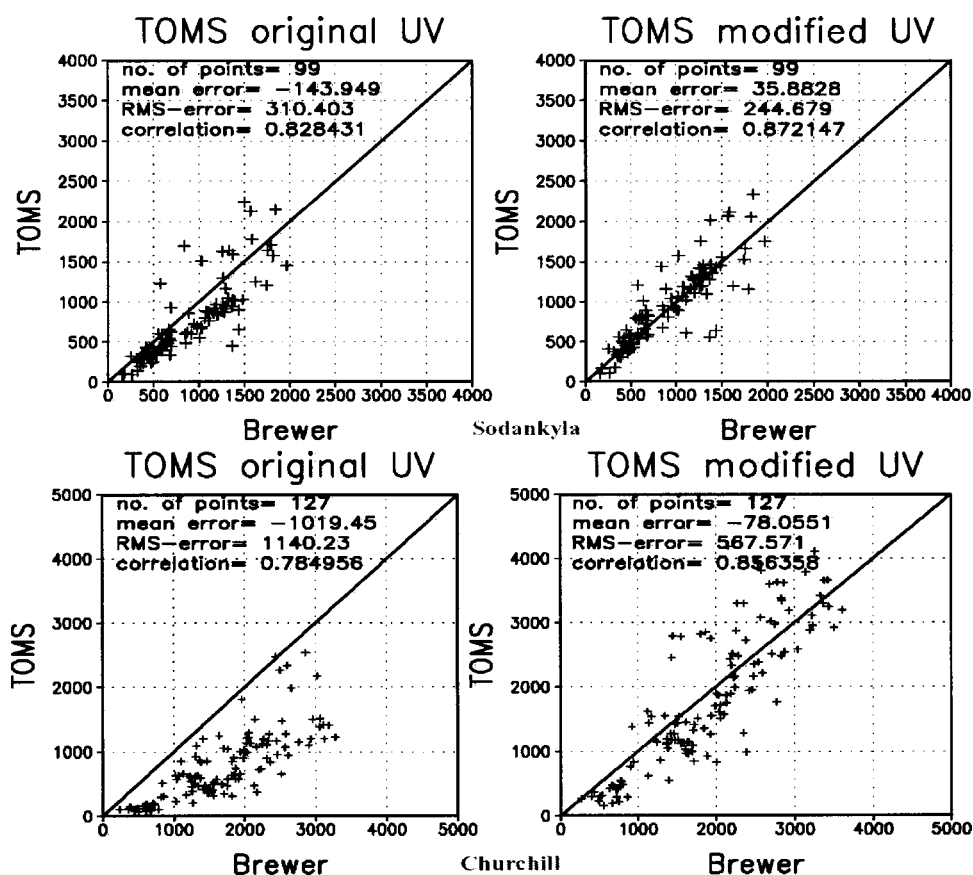


Fig. 5 The effect of the new snow albedo treatment on the computed surface UV. TOMS original UV is based on MLER^{60,61} whereas TOMS modified UV is based on the snow albedo regression with ERA-15 snow depth data, and coincident and collocated and colocated Nimbus 7 TOMS reflectivity measurements (covering the time period 1979 to 1994).⁶⁸ Top: comparison at Sodankylä, Finland; and bottom: Churchill, Canada.

UV radiation is more strongly attenuated by such aerosols than by nonabsorbing aerosols of the same optical depth. Moreover, since these aerosols also attenuate the outgoing radiation, the satellite algorithms that treat these aerosols as nonabsorbing underestimate their optical depth, amplifying the error further, causing overestimation of UV irradiance.^{27,41} This overestimation is proportional to the aerosol absorption optical thickness, which is a product of extinction optical thickness and single scattering co-albedo ($1 - \omega_0$). Though it is well known that mineral aerosols from the deserts and soot produced by biomass burning and urban transportation strongly absorb the UV radiation,^{27,31,69–74} properties of other potential UV absorbers, e.g., nitrated and aromatic aerosols,⁵⁶ are poorly known. To make matters worse, the distribution of UV-absorbing constituents of aerosols (iron-oxide, soot, nitrated inorganics, etc.) is highly variable, both in space and time, even within a large urban area.⁵⁶ Though satellite UV instruments can detect such aerosols when the conditions are right (absence of clouds, large elevated plumes), they typically miss them when the aerosols are located mostly in the planetary boundary layer. A correction scheme for the former aerosol types is described next.

When the absorbing aerosol plumes are transported into the free troposphere, they absorb the diffuse radiation emanating from lower altitudes and reaching the satellite. Since

the diffuse radiation, produced largely by molecular scattering, is a strong function of wavelength, the effect of such aerosols also varies with wavelength. In its simplest form they cause the satellite-derived LER to decrease with a decrease in wavelength, which can be used to detect the presence of such aerosols. (By contrast, nonabsorbing aerosols typically cause the LER to increase with decrease in wavelength, though this effect is usually quite small.) This is the basis for deriving the TOMS aerosol index (AI).^{75,76} Using this AI, one can construct a simple absorbing aerosol correction (AAC) algorithm^{27,31} as follows:

$$\frac{E_{\text{aerosol}}}{E_{\text{clear}}} = \exp(-g(H_A)AI), \quad (9)$$

where conversion factor g is a function of aerosol height H_A , observational geometry, and aerosol type. Radiative transfer calculations show that for the same altitude g factor is smaller for dust aerosol than for biomass burning smoke.⁴¹ Without discrimination between dust and smoke aerosol types, a compromise value of $g = 0.25$ was recommended as a first-order correction for tropical regions.²⁷ This value should be refined based on dust versus smoke discrimination techniques. Currently the TOMS aerosol algorithm employs a geographical approach for such dis-

Table 2 Expected errors in absorbing aerosol correction (AAC) method due to uncertainty in aerosol plume height 0.5 km for biomass burning smoke and dust.³¹ Aerosol models from Ref. 76.

Model/Parameter	Aerosol single scattering albedo at 324 nm	Error
Smoke C1	0.92	1.5%
Smoke C2	0.84	7.5%
Dust D1	0.90	1.7%
Dust D2	0.72	11%
Dust D3	0.63	16%

crimination, because the TOMS aerosol channels in the 330 to 380-nm range are not sufficiently separated to allow enough spectral contrast between these two aerosol types.⁷⁷ The information content of aerosol measurements from space will certainly be increased in the future by combining UV, visible, and near-IR channels of the advanced satellite sensors (MODIS, GOME, SCIAMATCHY, OMI) and exploiting additional radiation signatures (polarization, angular dependence).

For the AAC method, an additional problem arises from uncertainty in aerosol plume height. The current TOMS AAC algorithm assumes the nominal height of 3 km for plumes of desert dust and biomass burning smoke in the tropics.^{27,31} The uncertainty in the actual aerosol height is included in the error budget of the TOMS UV products as shown in Table 2.³¹ In the second version of the TOMS UV algorithm, the H_A could be estimated using the GSFC data assimilation winds in the GOCART model⁷⁸ or other sources.

Since AI is not sensitive to UV absorbers in the boundary layer, the AAC technique cannot correct for such aerosols. This may be the reason why the TOMS seems to overestimate surface UV in industrial/urban regions. Since there is very little understanding of the type and amount of UV absorbers that may be present in these areas, this problem currently remains unsolved.

6 Conclusions

We describe and evaluate the effects of enhancements to the current (Version 1) TOMS surface UV irradiance algorithm. The enhancements include a more detailed treatment of tropospheric aerosols, effects of diurnal variation of cloudiness, and an improved treatment of snow/ice. Some of the proposed improvements will be implemented in the second version of the TOMS UV algorithm after an extensive validation period (2002 to 2003). Validation of spatially averaged UV irradiance (satellite) with temporally averaged UV data (ground station) under broken cloud conditions would require implementation of special subsatellite UV validation campaigns and an optimal ground UV validation strategy. Use of the new algorithm will reduce the differences between ground-based and satellite estimations of UV irradiance and exposure.

7 Appendix: Cloud Shape Effects

The fractional cloud model described still ignores the 3-D cloud structure and related cloud-radiation effects (cloud shadows, reflection from nonhorizontal surfaces). Here we

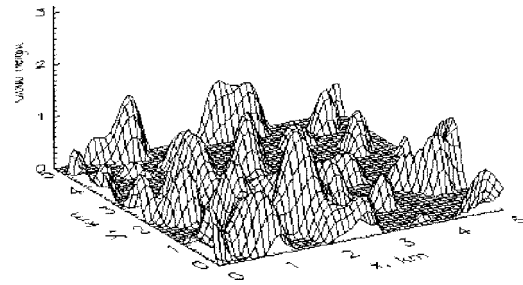


Fig. 6 Fragment of the broken cloud field as model input. The model is based on the normal random (Gaussian) field with a fixed lower boundary.⁷⁹ Spatially inhomogeneous cloud structure is described by a 3-D array of cells each with prescribed cloud properties. The dimensions of each cell should be sufficiently small compared to the photons free path. In most cases 50 to 100-m cells were found to be sufficient in modeling TOMS and OMI FOVs. The dimensions of the calculated field are similar to a single OMI FOV (10×20 km). Cloud cover 0.5, aspect ratio 1, scattering coefficient 50 km⁻¹, and cloud average diameter 1 km.

estimate some cloud shape errors on the FOV average cloud transmittance (C_T) using more detailed cloud models and a Monte-Carlo radiative transfer code.⁷⁹ Figure 6 shows one possible cloud model, which describes a fair weather cumulus cloud field. This cloud model relates stochastic field characteristics with cloud amount, mean cloud diameter, and aspect ratio. Based on these input parameters, a representation of a cloud field is constructed as a convolution of a 2-D Fourier series with random coefficients. Calculations of the radiance at the top of the atmosphere and irradiance at the surface are performed using a 3-D Monte-Carlo (MC) code.⁷⁹

Figure 7 shows the simulated normalized angular distribution of the 380-nm radiance at the top of the atmosphere (Anisotropic function, AIF⁸⁰) backscattered from the cloud scene shown in Fig. 6. The AIF angular distribution is slightly asymmetrical in the solar principal plane with larger relative reflection in the backscattering direction, where a satellite does not see any cloud shadows (hot spot). A different AIF angular distribution is assumed in the current TOMS UV algorithm, which results from the assumed plane-parallel C1 cloud model. The TOMS AIF has a relatively larger forward reflection and does not have a hot spot spike. It is the difference between the actual and TOMS assumed AIF_{TOMS}, that produces the error in cloud transmittance for estimation of surface irradiance. The correction factor is proportional to the AIF ratio: AIF_{actual}/AIF_{TOMS} averaged over TOMS FOV. It is a function of assumed cloud parameters, observational geometry, and surface albedo.

Figure 8 shows the correction factor for the cloud scene shown in Fig. 6. The factor should be applied to the standard C_T value calculated using the optically equivalent (i.e., providing the same UV reflectance in the satellite direction) homogeneous cloud model [see Eq. (2)]. As expected, the factor is maximal in the solar principal plane. For this particular cloud scene and $\theta_o = 54$ deg, the factor ranges from 0.85 ($\varphi = 0$ deg, forward reflecting) to 1.2 ($\varphi = 180$ deg, backward reflecting, i.e., hot spot).

Because the equatorial overpass occurs close to solar noon, the TOMS instrument scans in a direction that is

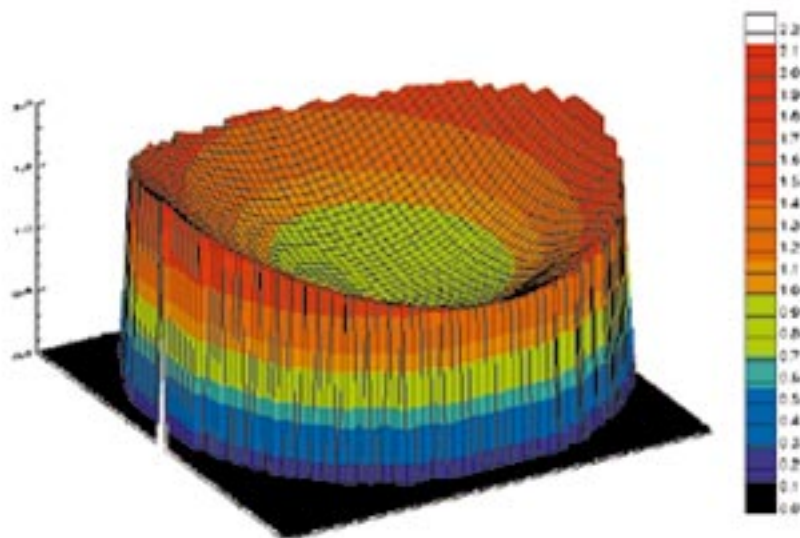


Fig. 7 Anisotropic function $AIF(\theta_0, \theta, \varphi)$ of the broken cloud scene (Fig. 6) for $\theta_0=54$ deg as a function of the satellite vertical angle θ (giving by distance from the center of the figure—nadir direction) and solar azimuthal angle, φ (given by polar angle: forward reflecting in on the right and backward reflecting on the left). The AIF is defined as the ratio of the equivalent Lambertian flux, $\pi L(\theta_0, \theta, \varphi)$, to the actual reflected flux, $M(\theta_0)$; $AIF = \pi L(\theta_0, \theta, \varphi) / M(\theta_0)$,⁸⁰ where $L(\theta_0, \theta, \varphi)$ is the satellite measured radiance at the top of the atmosphere. Representing reflectance to albedo ratio, the AIF is a direct measure of the angular anisotropy of the scene reflectance: $AIF < 1$ (shown by green color) means that the actual measured radiance is less than would be measured in the case of isotropic (Lambertian) scene reflectance with the same albedo. On the other hand, $AIF > 1$ (red colors) means that the actual measured radiance for a broken cloud scene is greater than those from the isotropic (Lambertian) scene with the same albedo.

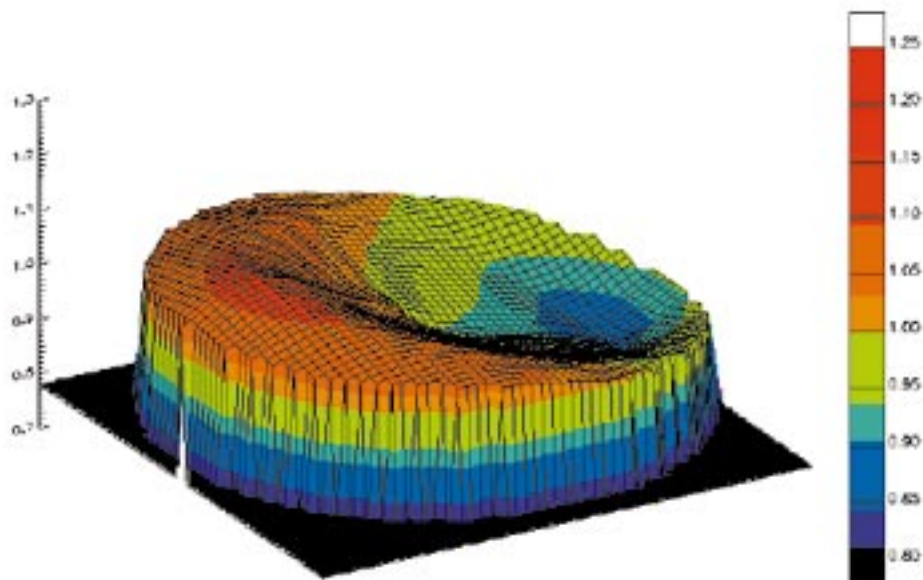


Fig. 8 Example of a correction factor for a broken cloud scene (Fig. 6), which should be applied to the satellite UV data calculated with the TOMS method (i.e., using a homogeneous plane-parallel cloud model). Depending on the satellite viewing direction (explained in Fig. 7), the correction factor ranges from 0.85 to 1.2. Cloud anisotropy is much less in the plane perpendicular to the solar principal plane than in the solar principal plane. Surface reflectivity is 5%. Solar zenith angle is 54 deg. The equivalent optical thickness of the homogeneous plane parallel cloud layer is close to 5.

approximately perpendicular to the principal plane of the sun. Figure 8 shows that for these directions the correction factor is much less than in the solar principal plane. However, the errors may be still significant for specific observational conditions (we found that the error increases with solar zenith angle, i.e., at high latitudes).

The same approach is being applied to quantify the errors due to an assumption of Lambertian snow reflection. To quantify the error, the Monte-Carlo radiative transfer model has to be run for a realistic snow bidirectional reflection distribution function (BRDF) to calculate the surface UV irradiance over snow with and without clouds. Preliminary calculations have shown that broken cloud effects over snow differ from uniform cloud effects over snow.

Acknowledgments

The work was supported by the NASA TOMS project.

References

1. R. S. Stolarski, P. Bloomfield, R. D. McPeters, and J. R. Herman, "Total ozone trends deduced from Nimbus 7 TOMS data," *Geophys. Res. Lett.* **18**, 1015–1018 (1991).
2. J. R. Herman and D. Larko, "Low ozone amounts during 1992 and 1993 from Nimbus 7 and Meteor 3 total ozone mapping spectrometers," *J. Geophys. Res., [Atmos.]* **99**, 3483–3496 (1994).
3. R. D. McPeters, S. M. Hollandsworth, L. E. Flynn, J. R. Herman, and C. J. Sefior, "Long-term ozone trends derived from the 16-year combined Nimbus 7/Meteor 3 TOMS Version 7 record," *Geophys. Res. Lett.* **23**, 3699–3702 (1996).
4. S. Madronich, "Implications of recent total ozone measurements for biologically active ultraviolet radiation reaching the Earth's surface," *Geophys. Res. Lett.* **19**, 37–40 (1992).
5. S. Madronich, "The atmosphere and UV-B Radiation at ground level," in *Environmental UV Photobiology*, A. R. Young, L. O. Bjorn, J. Moan, and W. Nultsch, Eds., pp. 1–39, Plenum Press, New York (1993).
6. A. F. Bais, C. S. Zerefos, C. Meleti, I. C. Ziomas, and K. Tourpali, "Spectral measurements of solar UVB radiation and its relations to total ozone, SO₂, and clouds," *J. Geophys. Res., [Atmos.]* **98**, 5199–5204 (1993).
7. R. L. McKenzie, M. Kotkamp, and W. Ireland, "Upwelling UV spectral irradiances and surface albedo measurements at Lauder, New Zealand," *Geophys. Res. Lett.* **23**, 1757–1760 (1996).
8. J. R. Herman, P. K. Bhartia, Z. Ahmad, and D. Larko, "UV-B radiation increases (1979–1992) from decreases in total ozone," *Geophys. Res. Lett.* **23**, 2117–2120 (1996).
9. V. E. Fioletov, J. B. Kerr, and D. I. Wardle, "The relationship between total ozone and spectral UV irradiance from Brewer observations and its use for derivation of total ozone from UV measurements," *Geophys. Res. Lett.* **24**, 2997–3000 (1997).
10. V. E. Fioletov and W. F. J. Evans, "The influence of ozone and other factors on surface radiation," in *Ozone Science: a Canadian Perspective on the Changing Ozone Layer*, D. I. Wardle, J. B. Kerr, C. T. McElroy, and D. R. Francis, Eds., CARD 97-3, pp. 73–90, Environment Canada Report (1997).
11. N. B. Chubarova, "Ultraviolet radiation under broken cloud conditions as inferred from many-year ground-based observations," *Izv. Akad. Nauk, Fiz. Atmos. Okeana* **34**, 131–135 (1998).
12. A. A. Sabziparvar, P. M. de F. Forster, and K. P. Shine, "Changes in ultraviolet radiation due to stratospheric and tropospheric ozone changes since preindustrial times," *J. Geophys. Res., [Atmos.]* **103**, 26107–26113 (1998).
13. J. R. Herman, R. L. McKenzie, S. B. Diaz, J. B. Kerr, S. Madronich, and G. Seckmeyer, "Ultraviolet radiation at the Earth's surface," Chap. 9 in *Scientific Assessment of Ozone Depletion: 1998, World Meteorological Organization (WMO98), Global Ozone Research and Monitoring Project*, Report No. 44, ISBN:92-807-1722-7, Geneva, Switzerland (1999).
14. "Effects of increased ultraviolet radiation in the Arctic, an interdisciplinary report on the state of knowledge and research need," International Arctic Science Committee (IASC), IASC Report N2, available from IASC Secretariat, Middelthuis Gate 29, P.O. Box 5072, Majorstua, 0301 Oslo, Norway (1996).
15. D. L. Leffell and D. E. Brash, "Sunlight and skin cancer," *Sci. Am.*, 52–59 (1996).
16. "Effects of increased ultraviolet radiation on biological systems," Scientific Committee on Problems of the Environment (SCOPE), 51 bd de Montmorency, 75016 Paris, France (1992).
17. "Effects of increased ultraviolet radiation on global ecosystems," Scientific Committee on Problems of the Environment (SCOPE), 51 bd de Montmorency, 75016 Paris, France (1993).
18. R. C. Smith, B. B. Prezelin, K. S. Baker, R. R. Biligare, N. P. Boucher, T. Coley, D. Karentz, S. MacIntyre, H. A. Matlic, D. Menzies, M. Ondrusek, Z. Wan, and K. J. Waters, "Ozone depletion: ultraviolet radiation and phytoplankton biology in Antarctic waters," *Science* **255**, 952–959 (1992).
19. "Ultraviolet radiation in Antarctica: Measurements and biological effects," C. S. Weiler and P. A. Penhale, Eds., AGU, *Antarctic Res. Series* **62**, 257 (1994).
20. "Environmental effects of stratospheric ozone depletion-1994 assessment," J. C. van der Leun, A. H. Teramura, and M. Tevini, Eds., United Nations Environment Programme (UNEP), Nairobi, Kenya (1994).
21. J. E. Frederick and D. Lubin, "The budget of biologically active ultraviolet radiation in the Earth-atmosphere system," *J. Geophys. Res., [Atmos.]* **93**(D4), 3825–3832 (1988).
22. D. Lubin, P. Ricchiazzi, C. Gautier, and R. H. Whritner, "A method for mapping Antarctic surface ultraviolet radiation using multispectral satellite imagery," in *Ultraviolet Radiation in Antarctica: Measurements and Biological Effects*, C. S. Weiler, and P. A. Penhale, Eds., AGU, *Antarctic Research Series* **62**, 53–82 (1994).
23. T. F. Eck, P. K. Bhartia, and J. B. Kerr, "Satellite estimation of spectral UVB irradiance using TOMS derived ozone and reflectivity," *Geophys. Res. Lett.* **22**, 611–614 (1995).
24. D. Lubin and E. H. Jensen, "Effects of clouds and stratospheric ozone depletion on ultraviolet radiation trends," *Nature (London)* **377**, 710–713 (1995).
25. C. S. Long, A. J. Miller, H. T. Lee, J. D. Wild, R. C. Przywarty, and D. Hufford, "Ultraviolet index forecasts issued by the National Weather Service," *Bull. Am. Meteorol. Soc.* **77**, 729–747 (1996).
26. R. Meerkoetter, B. Wissinger, and G. Seckmeyer, "Surface UV from ERS-2/GOME and NOAA/AVHRR data: A case study," *Geophys. Res. Lett.* **24**, 1939–1942 (1997).
27. N. A. Krotkov, P. K. Bhartia, J. R. Herman, V. Fioletov, and J. Kerr, "Satellite estimation of spectral surface UV irradiance in the presence of tropospheric aerosols 1. Cloud-free case," *J. Geophys. Res., [Atmos.]* **103**, 8779–8793 (1998).
28. D. Lubin, E. H. Jensen, and H. P. Gies, "Global surface ultraviolet radiation climatology from TOMS and ERBE data," *J. Geophys. Res., [Atmos.]* **103**, 26061–26091 (1998).
29. B. Mayer, C. A. Fischer, and S. Madronich, "Estimation of surface actinic flux from satellite (TOMS) ozone and cloud reflectivity measurements," *Geophys. Res. Lett.* **25**, 4321–4324 (1998).
30. P. Peeters, J. F. Muller, P. C. Simon, E. Celarier, and J. R. Herman, "Estimation of UV flux at the Earth's surface from GOME data," *ESA, Earth Observation* **58**, 39–40 (1998).
31. J. R. Herman, N. Krotkov, E. Celarier, D. Larko, and G. Labow, "The distribution of UV radiation at the Earth's surface from TOMS measured UV-backscattered radiances," *J. Geophys. Res., [Atmos.]* **104**, 12059–12076 (1999).
32. J. Verdebout, "A method to generate surface UV radiation maps over Europe using GOME, Meteosat, and ancillary geophysical data," *J. Geophys. Res., [Atmos.]* **105**, 5049–5058 (2000).
33. J. Matthijsen, H. Slaper, H. A. J. M. Reinen, and G. J. M. Velders, "Reduction of solar UV by clouds: Comparison between satellite-derived cloud effects and ground-based radiation measurements," *J. Geophys. Res., [Atmos.]* **105**, 5069–5080 (2000).
34. Z. Li, P. Wang, and J. Cihlar, "A simple and efficient method for retrieving surface UV radiation dose rate from satellite," *J. Geophys. Res., [Atmos.]* **105**, 5027–5036 (2000).
35. S. Kalliskota, "Some approaches to estimate UV radiation reaching the Earth's surface by using satellite data and their validation," Licentiate dissertation, Univ. of Helsinki (2001).
36. N. A. Krotkov, J. R. Herman, P. K. Bhartia, V. Fioletov, and Z. Ahmad, "Satellite estimation of spectral surface UV irradiance 2. Effects of homogeneous clouds and snow," *J. Geophys. Res., [Atmos.]* **106**, 11743–11759 (2001).
37. A. Arola, S. Kalliskota, P. N. den Outer, K. Edvardsen, G. Hansen, T. Koskela, T. J. Martin, J. Matthijsen, R. Meerkoetter, P. Peeters, G. Seckmeyer, P. Simon, H. Slaper, P. Taalas, and J. Verdebout, "Four UV mapping procedures using satellite data and their validation against ground-based UV measurements," *J. Geophys. Res., [Atmos.]* **107** (2002).
38. R. D. McPeters, P. K. Bhartia, A. J. Krueger, J. R. Herman, B. M. Schlessinger, C. G. Wellemeyer, C. J. Sefior, G. Jaross, S. L. Taylor, T. Swisler, O. Torres, G. Labow, W. Byerly, and R. P. Cebula, "Total ozone mapping spectrometer (TOMS) data products user's guide," NASA Ref. Publ. No 1384 (1996).
39. A. P. Vasilkov, N. Krotkov, J. R. Herman, C. McClain, K. Arrigo, and W. Robinson, "Global mapping of underwater UV irradiance and DNA-weighted exposures using TOMS and SeaWiFS data products," *J. Geophys. Res., [Oceans]* **106**, 27205–27219 (2001).

40. A. P. Vasilkov, J. R. Herman, N. Krotkov, G. Mitchell, and M. Kahru, "Problems of assessment of UV penetration into natural waters from space based measurements," *Opt. Eng.* **41**(12) (2002).
41. N. A. Krotkov, J. R. Herman, P. K. Bhartia, C. Seftor, A. Arola, J. Kaurola, P. Taalas, S. Kalliskota, and A. Vasilkov, "OMI surface UV irradiance algorithm," in *Ozone Monitoring Instrument (OMI) Algorithm Theoretical Basis Document, vol. 3, Aerosol, Clouds and Surface UV Irradiance*, P. Stammes, Ed., KNMI (2002).
42. N. Chubarova, A. Y. Yurova, N. A. Krotkov, Jay R. Herman, and P. K. Bhartia, "Comparisons between ground measurements of UV irradiance 290 to 380 nm and TOMS UV estimates over Moscow for 1979–2000," *Opt. Eng.* **41**(12) (2002).
43. J. Slusser, J. R. Herman, W. Gao, N. A. Krotkov, G. Labow, and G. Scott, "Comparison of USDA UV shadowband irradiance measurements with TOMS satellite retrievals and DISORT model under all sky conditions," *Proc. SPIE* **4482**, 56–69 (2002).
44. V. E. Fioletov, J. B. Kerr, D. I. Wardle, N. A. Krotkov, and J. R. Herman, "Comparison of Brewer UV irradiance measurements with TOMS satellite retrievals," *Opt. Eng.* **41**(12) (2002).
45. R. L. McKenzie, G. Seckmeyer, A. F. Bais, J. B. Kerr, and S. Madronich, "Satellite retrievals of erythemal UV dose compared with ground-based measurements at northern and southern midlatitudes," *J. Geophys. Res.* **106**, 24051–24062 (2001).
46. S. Kalliskota, J. Kaurola, P. Taalas, J. R. Herman, E. A. Celarier, and N. Krotkov, "Comparison of daily UV doses estimated from Nimbus 7/TOMS measurements and ground-based spectroradiometric data," *J. Geophys. Res., [Atmos.]* **105**, 5059–5067 (2000).
47. G. E. Brueckner, et al., "The solar ultraviolet spectral irradiance monitor (SUSIM) on board the upper atmospheric research satellite (UARS)," *J. Geophys. Res., [Atmos.]* **98**, 10695–10711 (1993).
48. G. J. Rottman, et al., "Solar stellar irradiance comparison experiment 1 I: instrument design and operation," *J. Geophys. Res., [Atmos.]* **98**, 10667–10678 (1993).
49. R. P. Cebula, et al., "Observations of the solar irradiance in the 200–350 nm interval during the ATLAS-1 mission: A comparison among three sets of measurements—SSBUV, SOLSPEC, and SUSIM," *Geophys. Res. Lett.* **23**, 289–292 (1996).
50. T. N. Woods, et al., "Validation of the UARS solar ultraviolet irradiances: Comparison with the ATLAS 1 and 2 measurements," *J. Geophys. Res., [Atmos.]* **101**, 9541–9569 (1996).
51. S. C. Liu, S. A. McKeen, and S. Madronich, "Effect of anthropogenic aerosols on biologically active ultraviolet radiation," *Geophys. Res. Lett.* **18**, 2265–2268 (1991).
52. R. R. Dickerson, S. Kondragunta, G. Stenichikov, K. L. Civerolo, B. G. Doddridge, and B. N. Holben, "The impact of aerosols on solar ultraviolet radiation and photochemical smog," *Science* **278**, 827–830 (1997).
53. C. J. Erlick, J. E. Frederick, V. K. Saxena, and B. N. Wenny, "Atmospheric transmission in the ultraviolet and visible: aerosols in cloudy atmospheres," *J. Geophys. Res., [Atmos.]* **103**, 31541–31556 (1998).
54. C. J. Erlick and J. E. Frederick, "Effects of aerosols on the wavelength dependence of atmospheric transmission in the ultraviolet and visible 2. Continental and urban aerosols in clear skies," *J. Geophys. Res., [Atmos.]* **103**, 23275–23285 (1998).
55. A. Kylling, A. F. Bais, M. Blumthaler, J. Schreder, C. S. Zerefos, and E. Kosmidis, "Effect of aerosols on solar UV irradiance during the photochemical activity and solar ultraviolet radiation campaign," *J. Geophys. Res., [Atmos.]* **103**, 26051–26060 (1998).
56. M. Z. Jacobson, "Isolating nitrated and aromatic aerosols and nitrated aromatic gases as sources of ultraviolet light absorption," *J. Geophys. Res., [Atmos.]* **104**, 3527–3542 (1999).
57. W. J. Wiscombe and S. G. Warren, "A model for the spectral albedo of snow, I. Pure snow," *J. Atmos. Sci.* **37**, 2712–2733 (1980).
58. T. C. Grenfell, S. G. Warren, and P. C. Mullen, "Reflection of solar radiation by the Antarctic snow surface at ultraviolet, visible, and near-infrared wavelengths," *J. Geophys. Res., [Atmos.]* **99**, 18669–18684 (1994).
59. J. Lenoble, "Modeling of the influence of snow reflectance on ultraviolet irradiance for cloudless sky," *Appl. Opt.* **37**, 2441–2447 (1998).
60. J. R. Herman and E. Celarier, "Earth surface reflectivity climatology at 340 to 380 nm from TOMS data," *J. Geophys. Res., [Atmos.]* **102**, 28003–28011 (1997).
61. J. R. Herman, E. Celarier, and D. Larko, "UV 380 nm reflectivity of the Earth's surface, clouds and aerosols," *J. Geophys. Res., [Atmos.]* **106**, 5335–5351 (2001).
62. Z. Ahmad, J. R. Herman, P. K. Bhartia, A. P. Vasilkov, N. A. Krotkov, C. Hsu, C. Seftor, and M. Tzortziou, "Spectral dependence and chlorophyll signatures in TOMS minimal reflectivity data over oceans," *J. Geophys. Res. [Oceans]* (to be published).
63. D. Deirmendjian, *Electromagnetic Scattering on Spherical Polydispersions*, p. 290, Elsevier Publishing Company, New York (1969).
64. W. B. Rossow and R. A. Schiffer, "ISCCP cloud data products," *Bull. Am. Meteorol. Soc.* **72**, 2–20 (1991).
65. M. L. Nack and A. E. S. Green, "Influence of clouds, haze and smog on the middle ultraviolet reaching the ground," *Appl. Opt.* **13**, 2405–2415 (1974).
66. M. Blumthaler and W. Ambach, "Solar UVB-albedo of various surfaces," *Photochem. Photobiol.* **48**, 85–88 (1988).
67. B. L. Diffey, A. T. Green, M. J. Loftus, G. J. Johnston, and P. S. Lee, "A portable instrument for measuring ground reflectance in the ultraviolet," *Photochem. Photobiol.* **61**, 68–70 (1995).
68. A. Arola, J. Kaurola, L. Koskinen, A. Tanskanen, T. Tikkanen, P. Taalas, J. R. Herman, N. Krotkov, and V. Fioletov "A new approach to estimate the albedo for snow-covered surface in space-borne UV retrieval method," (to be published).
69. B. N. Holben, et al., "AERONET-A federated instrument network and data archive for aerosol characterization," *Remote Sens. Environ.* **66**, 1–16 (1998).
70. B. N. Holben, et al., "An emerging ground-based aerosol climatology: aerosol optical depth from AERONET," *J. Geophys. Res., [Atmos.]* **106**, 12067–12097 (2001).
71. A. Smirnov, et al., "Optical properties of atmospheric aerosol in maritime environments," *J. Atmos. Sci.* **59**, 501–523 (2002).
72. O. Dubovik, et al., "Variability of absorption and optical properties of key aerosol types observed in worldwide locations," *J. Atmos. Sci.* **59**, 590–608 (2002).
73. Eck, et al., "Measurements of irradiance attenuation and estimation of aerosol single scattering albedo for biomass burning aerosols in Amazonia," *J. Geophys. Res., [Atmos.]* **103**, 31865–31878 (1998).
74. Eck, et al., "Characterization of the optical properties of biomass burning aerosols in Zambia during the 1997 ZIBBEE field campaign," *J. Geophys. Res., [Atmos.]* **106**, 3425–3448 (2001).
75. J. R. Herman, P. K. Bhartia, O. Torres, C. Hsu, C. Seftor, and E. Celarier, "Global distribution of UV-absorbing aerosols from Nimbus-7/TOMS data," *J. Geophys. Res., [Atmos.]* **102**, 16911– (1997).
76. O. Torres, P. K. Bhartia, J. R. Herman, and Z. Ahmad, "Derivation of aerosol properties from satellite measurements of backscattered ultraviolet radiation. Theoretical basis," *J. Geophys. Res., [Atmos.]* **103**, 17099–17110 (1998).
77. O. Torres, P. K. Bhartia, J. R. Herman, A. Sinyuk, P. Ginoux, and B. Holben, "A long-term record of aerosol optical depth from TOMS observations and comparison to AERONET measurements," *J. Atmos. Sci.* **59**, 398–413 (2002).
78. M. Chin, P. Ginoux, S. Kinne, O. Torres, B. N. Holben, B. N. Duncan, R. V. Martin, J. F. Logan, A. Higuerashi, and T. Nakajima, "Tropospheric aerosol optical thickness from the GOCART model and comparisons with satellite and sun photometer measurements," *J. Atmos. Sci.* **59**, 461–483 (2002).
79. I. V. Geogdzhayev, T. V. Kondranin, A. N. Rublev, and N. Y. Chubarova, "UV radiation transfer through broken cloud fields modeling and comparison with measurements," *Izv. Akad. Nauk, Fiz. Atmos. Okeana* **33**(5), 630–635 (1997).
80. J. T. Suttles, R. N. Green, G. L. Smith, B. A. Wielicki, I. J. Walker, V. R. Taylor, and L. L. Stowe, "Angular radiation models for the Earth-atmosphere system. Vol. 1 Shortwave radiation," pp. 159, NASA reference publication RP-1184, (1989).



Nickolay Krotkov received a BS from Moscow Institute of Physics and Technology in physics in 1983, a MS (with honor) in remote sensing in 1985, and a PhD in oceanography (physics and mathematics) in 1990 from the P. P. Shirshov Institute of Oceanology, Russian Academy of Sciences, where his major research was using polarization properties of light in oceanic remote sensing. He joined NASA, Goddard Space Flight Center, with a University Space Research Association postdoctoral appointment in 1993, where he has since been engaged in development of applications of satellite data, such as ultraviolet (UV) irradiance estimation at the Earth's surface and underwater as well as generation of volcanic eruption data products from the NASA Total Ozone Mapping Spectrometer (TOMS) missions. His main field of research is radiative transfer modeling and satellite- and ground-based UV data analysis. He is currently a senior research scientist with Goddard Earth Sciences and Technology Center, University of Maryland Baltimore County, working on new product algorithms for hyperspectral satellite imagers, such as the Ozone Monitoring Instrument (OMI) on the NASA EOS/Aura satellite.



Jay Herman received his BS degree in 1959 (Clarkson), and MS (1963) and PhD (1965) in physics and aeronomy from Pennsylvania State University. He joined NASA, Goddard Space Flight Center, first with a National Academy of Sciences post-doctoral appointment and then as a staff scientist. Dr. Herman has worked in a number of fields including chemical modeling of the Earth and planetary atmospheres, radiative transfer, satellite data studies of

ozone, clouds, surface reflectivity, and UV radiation in the atmosphere and oceans. He currently is project scientist on the Deep Space Climate Observatory at the Lagrange-1 observing point. He is also principal investigator on the Earth UV radiation project. Dr. Herman is a long-term member of the American Geophysical Union.



Jussi Kaurola received the MSc degree in 1988 and the PhD degree in 1996 in meteorology from the University of Helsinki, Finland. His research work has been focused on several aspects of solar UV radiation, mainly in the area of long-term changes in UV, and data processing and analysis of ground-based UV measurements. He is a member of the ozone and UV research group at the Finnish Meteorological Institute.



Pawan K. Bhartia received his PhD in physics and MS in computer science in 1977 from Purdue University, West Lafayette, Indiana. Since then he has been associated with NASA's Goddard Space Flight Center (GSFC) in Greenbelt, Maryland. Between 1977 and 1991 he worked with several private companies (Systems & Applied Sciences Corp., STX, SAR, Interferometrics & TRW) on NASA contracts. Since October 1991 he has been a NASA employee. Currently he is the head of the Atmospheric Chemistry & Dynamics Branch at GSFC. He is also the project scientist of NASA's Total Ozone Mapping Spectrometer (TOMS) satellite mission and the U.S. science team leader of the Ozone Monitoring Instrument (OMI)—a joint project between NASA and The Netherlands. He has over 50 publications in UV remote sensing of the Earth from satellites, dealing principally with the measurement of the Earth's ozone layer. He is a member of the American Geophysical Union.

He is also the project scientist of NASA's Total Ozone Mapping Spectrometer (TOMS) satellite mission and the U.S. science team leader of the Ozone Monitoring Instrument (OMI)—a joint project between NASA and The Netherlands. He has over 50 publications in UV remote sensing of the Earth from satellites, dealing principally with the measurement of the Earth's ozone layer. He is a member of the American Geophysical Union.



Sari Kalliskota received the MSc degree in geophysics from the University of Oulu, Faculty of Science, in 1997 and the post-graduate degree of licentiate in philosophy in 2001. The subject of the licentiate thesis was "Some approaches to estimate UV radiation reaching the Earth's surface by using satellite data and their validation."



Petteri Taalas received the MSc degree in 1988 and the PhD degree in 1993 in meteorology at the University of Helsinki, Finland. He has worked at the Finnish Meteorological Institute since 1983. His current appointment is research professor and he is the head of the ozone and UV research group. He has 17 years of experience in atmospheric chemistry and meteorology. His research work has been focused on several aspects of remote sensing of the atmosphere, stratospheric ozone chemistry, and solar UV radiation. He has been a member of European Union Science Panel on Stratospheric Ozone since 1997, and a member of World Meteorological Organization Scientific Advisory Group on UV Radiation (UV SAG) since 1995.

He has been a member of European Union Science Panel on Stratospheric Ozone since 1997, and a member of World Meteorological Organization Scientific Advisory Group on UV Radiation (UV SAG) since 1995.



Colin Seftor has had over 10 years of experience in the design and development of algorithms for the retrieval of atmospheric constituents from UV and visible satellite measurements. He helped design, test, and implement the Version 7 total column ozone retrieval algorithm used with the Total Ozone Mapping Spectrometer (TOMS) sensors and he recently completed developing an improved version of the UV surface flux algorithm that will be used with

the Ozone Monitoring Instrument (OMI) as well as TOMS. He also helped to develop techniques to detect the location and track the movement of tropospheric aerosols using UV satellite measurements. He is currently working on designing and validating the performance of an improved total column ozone retrieval algorithm for use with the Ozone Mapping and Profiler Suite (OMPS), which is the next-generation ozone monitoring sensor that will be flown on the National Polar-orbiting Operational Environmental Satellite System (NPOESS).



Igor V. Geogdzhayev received his MS degree in remote sensing in 1993 and his PhD degree in physics in 1997 from Moscow Institute of Physics and Technology. During 1997 to 1998 he was a postdoctoral visiting scientist at State University of New York at Stony Brook and NASA Goddard Institute for Space Studies (GISS), New York City. He is currently with the Department of Applied Physics and Applied Mathematics at Columbia University/NASA

GISS. He has expertise in radiative transfer in inhomogeneous atmospheres, remote sensing of aerosols and clouds, and effects of broken cloudiness. He has developed a 3-D Monte Carlo code for radiative transfer calculations in inhomogeneous cloudy atmospheres and is currently working on NASA's Global Aerosol Climatology Project.



Antti Arola received the MSc degree in engineering from the Helsinki University of Technology, Espoo, Finland, in 1991 and the Phil. Lic. degree in meteorology from the University of Helsinki, Helsinki, Finland, in 1999. His research work has been focused on several aspects of solar UV radiation, mainly in the area of satellite-based UV and analysis of ground-based UV measurements. He is a member of the ozone and UV research group at the Finnish Meteorological Institute.

He is a member of the ozone and UV research group at the Finnish Meteorological Institute.